INAF
ISTITUTO NAZIONALE
DI ASTROFISICA
NATIONAL INSTITUTE
FOR ASTROPHYSICS



| | |
|---|---|
| ***Publication Year*** | 2023 |
| ***Acceptance in OA*** | 2025-02-25T12:09:36Z |
| ***Title*** | AF Lep b: The lowest-mass planet detected by coupling astrometric and direct imaging data |
| ***Authors*** | MESA, Dino, GRATTON, Raffaele, Kervella, P., Bonavita, M., DESIDERA, Silvano, D'ORAZI, VALENTINA, Zurlo, A., RIGLIACO, Elisabetta, Marino, Sebastian |
| ***Publisher's version (DOI)*** | 10.1051/0004-6361/202345865 |
| ***Handle*** | http://hdl.handle.net/20.500.12386/36201 |
| ***Journal*** | ASTRONOMY & ASTROPHYSICS |
| ***Volume*** | 672 |

A&A 672, A93 (2023)
https://doi.org/10.1051/0004-6361/202345865
© The Authors 2023

Astronomy & Astrophysics

# AF Lep b: The lowest-mass planet detected by coupling astrometric and direct imaging data⋆,⋆⋆

D. Mesa[1], R. Gratton[1], P. Kervella[2], M. Bonavita[3,1], S. Desidera[1], V. D'Orazi[4,1], S. Marino[5], A. Zurlo[6,7,8], and E. Rigliaco[1]

[1] INAF-Osservatorio Astronomico di Padova, Vicolo dell'Osservatorio 5, 35122 Padova, Italy
e-mail: dino.mesa@inaf.it
[2] LESIA, Observatoire de Paris, Université PSL, CNRS, Sorbonne Université, Université Paris-Cité, 5 place Jules Janssen, 92195 Meudon, France
[3] School of Physical Sciences, The Open University, Walton Hall, Milton Keynes MK7 6AA, UK
[4] Dipartimento di Fisica, Università di Roma Tor Vergata, Via della ricerca scientifica 1, 00133 Roma, Italy
[5] School of Physics and Astronomy, University of Exeter, Stocker Road, Exeter, EX4 4QL, UK
[6] Instituto de Estudios Astrofísicos, Facultad de Ingeniería y Ciencias, Universidad Diego Portales, Av. Ejército 441, Santiago, Chile
[7] Escuela de Ingeniería Industrial, Facultad de Ingeniería y Ciencias, Universidad Diego Portales, Av. Ejército 441, Santiago, Chile
[8] Millennium Nucleus on Young Exoplanets and their Moons (YEMS), Av. Ejército 441, Santiago, Chile

Received 9 January 2023 / Accepted 13 February 2023

**ABSTRACT**

*Aims.* Using the direct-imaging technique, we searched for low-mass companions around the star AF Lep, which presents a significant proper-motion anomaly (PMa) signal obtained from the comparison of HIPPARCOS and *Gaia* eDR3 catalogs.
*Methods.* We observed AF Lep in two epochs with VLT/SPHERE using its subsystems IFS and IRDIS in the near-infrared, covering wavelengths ranging from the Y to the K spectral bands (between 0.95 and 2.3 μm). We then reduced the data using the high-contrast imaging techniques angular differential imaging (ADI) and spectral differential imaging in order to be able to retrieve the signal from low-mass companions of the star.
*Results.* A faint companion was retrieved at a separation of ∼0.335″ from the star and with a position angle of ∼70.5° in the first epoch and with a similar position in the second epoch. This corresponds to a projected separation of ∼9 au. The extracted photometry allowed us to estimate a mass for the companion of between 2 and 5 $M_{\rm Jup}$. This mass is in good agreement with astrometric measurements of the dynamic mass of the companion, which give 5.2–5.5 $M_{\rm Jup}$. This is the first companion with a mass well below the deuterium burning limit that was discovered by coupling direct imaging with PMa measurements. Orbital fitting done using the orvara tool allowed us to further confirm the companion mass and to define its main orbital parameters.

**Key words.** instrumentation: spectrographs – methods: data analysis – techniques: imaging spectroscopy – planetary systems – stars: individual: AF Lep

## 1. Introduction

In the last decade or so, mainly thanks to the new generation of dedicated planet-finders like VLT/SPHERE (Beuzit et al. 2019), the Gemini Planet Imager (GPI; Macintosh et al. 2014), and Subaru/CHARIS (Groff et al. 2015), the number of directly imaged (DI) substellar companions has seen a rapid growth. Mainly made up of wide companions to young nearby stars, this population spans a wide range of masses from planetary companions to more massive brown dwarf companions. Some examples of planetary mass companions are 51 Eri b (Macintosh et al. 2015), HIP 65426 b (Chauvin et al. 2017b), and PDS 70 b and c (Keppler et al. 2018; Haffert et al. 2019). The vast majority of these discoveries comes from large, blind surveys, which have contributed to a first characterization of the young substellar population, highlighting a paucity of massive planets and brown dwarf companions at separations of larger than 10 au (Nielsen et al. 2019; Vigan et al. 2021), with an expected frequency of ∼5%−6%. Blind DI surveys, such as SHINE, which was performed using VLT/SPHERE (Chauvin et al. 2017a; Desidera et al. 2021; Langlois et al. 2021; Vigan et al. 2021), therefore come at a high cost in terms of telescope time, with a relatively low return in terms of new detections.

Our understanding of these objects therefore remains severely limited by the small number of known systems. In particular, the current sparse sample of DI companions shows a large diversity of spectrophotometric characteristics and orbital configurations, challenging to grasp them as a single populations. Larger numbers of detections are therefore essential in order to obtain a clearer picture of the formation patterns of substellar companions. As a result, more recent campaigns are using careful preselection methods to maximize the detection yield in the shortest amount of time. Recently, some success was achieved in directly imaging companions previously detected through radial velocity (RV), as in the case of $\beta$ Pic c (Nowak et al. 2020) and HD 206893 c (Hinkley et al. 2023). Other very

⋆ The spectrum is also available at the CDS via anonymous ftp to cdsarc.cds.unistra.fr (130.79.128.5) or via https://cdsarc.cds.unistra.fr/viz-bin/cat/J/A+A/672/A93

⋆⋆ Based on observations made with the European Southern Observatory (ESO) telescopes at the Paranal Observatory in Chile under the program 0110.C-0233(A).



Open Access article, published by EDP Sciences, under the terms of the Creative Commons Attribution License (https://creativecommons.org/licenses/by/4.0), which permits unrestricted use, distribution, and reproduction in any medium, provided the original work is properly cited.
This article is published in open access under the Subscribe to Open model. Subscribe to A&A to support open access publication.

successful programs have been those targeting stars showing proper-motion anomalies (PMas; often referred to as $\Delta\mu$, or astrometric accelerations). These values are obtained by searching for significant differences between proper motions measured over a long time baseline (e.g., *Tycho*-2, or *Tycho Gaia* Astrometric Solution – TGAS) and short-term proper motions, such as those measured by HIPPARCOS and *Gaia*. Several catalogs listing stars with PMas obtained by comparing HIPPARCOS data with those from both *Gaia* DR2 and eDR3 data are currently available (see e.g., Brandt 2018, 2021; Kervella et al. 2019, 2022) and have been used as a starting point for new targeted surveys, which have led to the discovery of several interesting companions, including HIP 21152 B, the first bound brown dwarf companion detected in the Hyades (Bonavita et al. 2022; Franson et al. 2023a), and the most recent discovery of a 13–16 $M_{\rm Jup}$ mass companion imaged around the accelerating star HIP 99770 (Currie et al. 2022). Recently, the results of the COPAINS survey were published by Bonavita et al. (2022), showing a substellar detection rate of ∼20%, providing definitive proof of the efficiency of the method.

We exploited the catalog presented in Kervella et al. (2022), which was obtained by comparing HIPPARCOS and *Gaia* eDR3 (Gaia Collaboration 2021) to select targets to be observed with VLT/SPHERE. The first selection criterion was that the PMa signal had a signal-to-noise ratio (S/N) of higher than 3 and lower than 10 in order to be sure to exclude stars with signals due to the presence of stellar mass companions. Moreover, we selected stars at less than 50 pc from the Sun in order to be able to image the inner part of the planetary system. Finally, we selected stars with young ages according to the literature (less than a few hundred million years) in order to ensure that the companion is bright enough to be imaged with SPHERE.

In this paper, we present a new Jupiter analog discovered with SPHERE around the accelerating star AF Lep, part of the Beta Pictoris Moving Group (BPMG). In Sect. 2, we present a detailed characterization of the host star, while Sect. 3 includes a description of the observations and data reduction. The results, including a spectral and orbital characterization of the companion, are presented in Sect. 4 and discussed in Sect. 5. Finally, in Sect. 6 we presents the conclusions of this study and its implications.

An independent and contemporaneous discovery of this companion is presented in De Rosa et al. (2023) and in Franson et al. (2023b).

## 2. Host-star properties

AF Lep (HIP 25486; HD 35850) is an F8 star (Gray et al. 2006) at a distance of 26.8 pc from the Sun (Gaia Collaboration 2023). It is part of the BPMG (Pawellek et al. 2021) with an estimated age of 24 ± 3 Myr (Bell et al. 2015), and hosts a debris disk with an estimated belt radius of 54 ± 6 au that is not yet resolved (Pawellek et al. 2021). Kervella et al. (2022) found a strong PMa signal for this star with a S/N of 8.99, making it an ideal target for our program.

Other main characteristics of AF Lep, including the PMa values from Kervella et al. (2022), are summarised in Table 1. This star was classified as a spectroscopic binary (SB2 star) with a stellar companion at a separation of 0.021 au (Nordström et al. 2004; Eker et al. 2008) and a mass ratio of 0.715. The binarity of the host star is an important point to be discussed, as the dynamical mass determined for a possible companion to AF Lep is proportional to the total mass assumed for the star, and this is different if it is a single or a multiple object. A discussion of this aspect is therefore crucial to the accurate interpretation of the available PMa data.

**Table 1.** Stellar parameters of AF Lep with references, including the HIP-EDR3 proper motion anomaly (PMa) and the corresponding tangential velocity anomaly ($dV_t$) with its position angle ($dV_t$ PA).

| Parameter | Value | Ref. |
|---|---|---|
| Sp. type | F8 V | 1 |
| $T_{\rm eff}$ (K) | 6100 | 2 |
| $\log g$ | 4.4 | 2 |
| B-V | 0.55 | 2, 3 |
| $v \sin i$ (km s$^{-1}$) | 54.7 ± 0.5 | 4 |
| Mass ($M_\odot$) | 1.20 ± 0.06 | 5 |
| Radius ($R_\odot$) | 1.25 ± 0.06 | 6 |
| Period (days) | 0.966 ± 0.002 | 7 |
| RV (km s$^{-1}$) | 21.10 ± 0.37 | 8 |
| Parallax (mas) | 37.253 ± 0.019 | 8 |
| Proper motion (mas yr$^{-1}$) | $\mu_\alpha$ = 16.915 ± 0.018 | 8 |
| | $\mu_\delta$ = −49.318 ± 0.016 | |
| PMa (mas yr$^{-1}$) | $\Delta\mu_\alpha$ = −0.206 ± 0.021 | 9 |
| | $\Delta\mu_\delta$ = −0.152 ± 0.019 | |
| $dV_t$ (m s$^{-1}$) | 32.60 ± 3.63 | 9 |
| $dV_t$ PA (°) | 233.50 ± 4.38 | |
| *Gaia* photometry: | G: 6.209 ± 0.002 | 8 |
| | BP: 6.488 ± 0.004 | |
| | RP: 5.752 ± 0.005 | |
| UBVRI photometry | B: 6.832 ± 0.015 | 10 |
| | V: 6.295 ± 0010 | |
| 2MASS photometry | J: 5.268 ± 0.027 | 11 |
| | H: 5.087 ± 0.026 | |
| | K: 4.926 ± 0.021 | |

**References.** (1) Eggen (1986); (2) Tagliaferri et al. (1994); (3) Cutispoto et al. (1996); (4) Marsden et al. (2014); (5) Kim & Demarque (1996); (6) Blackwell & Lynas-Gray (1994); (7) Järvinen et al. (2015); (8) Gaia Collaboration (2023); (9) Kervella et al. (2022); (10) Høg et al. (2000); (11) Cutri et al. (2003).

We first notice that no indication of binarity is present in *Gaia* DR3 as the star has a renormalised unit weight error (RUWE[1]) parameter of 0.918, which is compatible with a single source. Moreover, no hints of a companion are seen in Doppler imaging data by Järvinen et al. (2015). In addition, a nearly equal-mass binary suggested by the SB2 classification should produce a RV signal with an amplitude of several km s$^{-1}$, while no RV variation was found by Butler et al. (2017), who obtained a precision of ∼200 m s$^{-1}$ over a baseline of ∼20 yr. Also, the analysis of TESS photometry shows a periodogram with a single strong peak at 1.008 days. This value is very close to the photometric period of 0.996 days given by Messina et al. (2017) and Järvinen et al. (2015), with the small difference between the values likely due to aliasing. The expected period for a star belonging to the BPMG is below 10 days (Messina et al. 2017). We would therefore also expect the secondary to rotate at this rate and the peak to be visible in the TESS periodogram. Nevertheless, no additional peak is observed with a period below 10 days, which clearly disfavors any hypothesis that this star is

[1] The RUWE is a statistical indicator that can be used to assess the quality and reliability of *Gaia*'s astrometric data. Data compatible with a single-star model will have a RUWE of around 1, while a significantly higher value indicates a nonsingle or otherwise problematic source.

**Table 2.** List and main characteristics of the SPHERE observations of AF Lep used for this work.

| Date | Obs. mode | Coronograph | DIMM seeing | $\tau_0$ | Wind speed | Field rot. | DIT | Tot. exp. |
|---|---|---|---|---|---|---|---|---|
| 2022-10-16 | IRDIFS_EXT | N_ALC_YJH_S | 0.55″ | 5.8 ms | 7.35 m s$^{-1}$ | 13.3° | 32 s | 3584 s |
| 2022-12-20 | IRDIFS_EXT | N_ALC_YJH_S | 1.05″ | 4.0 ms | 8.82 m s$^{-1}$ | 51.8° | 32 s | 3584 s |

a SB2. The BVGJHK photometry of AF Lep is fully compatible with a star that is intermediate between an F8V and an F9V according to Pecaut & Mamajek (2013) and there is no indication for a luminosity excess, as would be expected for an SB2 system. The values of $v \sin i = 50.32$ km s$^{-1}$ and $P_{\rm rot} = 0.966$ days (Järvinen et al. 2015) are reasonably compatible (though slightly slower) with the color of the star as belonging to the BPMG. Interferometric observations by Evans et al. (2012) exclude the presence of companions with masses as high as 75 $M_{\rm Jup}$ at a separation of greater than 40 mas, and 33 $M_{\rm Jup}$ at a separation of greater than 80 mas. Moreover, given the inclination of 50 degrees (Marsden et al. 2006), which is fully compatible with observed $v \sin i$ and $P_{\rm rot}$, the RV variations seen by Nordström et al. (2004) are not compatible with a synchronized system. Finally, if the system has an inclination of 50 degrees and a mass ratio of 0.715, an amplitude of RV of ∼6 km s$^{-1}$, as indicated by the rms of Nordström et al. (2004), would require a semi-major axis of ∼13 au, that is ∼0.49″, and a period of ∼36 yr. This can be excluded by the lack of detection in existing high-contrast imaging and would also be incompatible with the measured PMa.

We therefore conclude that the classification as an SB2 by Nordström et al. (2004) is likely to be an artifact due to the presence of spots that altered the line profile in their observation and that AF Lep is a single star of spectral type between F8 and F9. The value of the stellar mass adopted in the remainder of our discussion is therefore around 1.20 $M_\odot$ (see Table 1), which is in agreement with the estimate given by Kervella et al. (2022).

## 3. Observations and data reduction

Table 2 summarizes the main characteristics of the SPHERE/SHINE observations of AF Lep, which were performed on October 16, 2022, and December 20, 2022. The weather conditions were good for the first epoch, but the target was observed far from the meridian, resulting in a very low field-of-view (FOV) rotation angle. The object was observed while passing at the meridian for the second epoch, but in slightly poorer weather conditions, with the seeing worsening during the second part of the observation.

Both observations made use of the SPHERE IRDIFS_EXT observing mode, with IFS (Claudi et al. 2008) covering a spectral range of between 0.95 and 1.65 µm (Y, J, and H spectral bands) and a FOV of 1.7″ × 1.7″, and IRDIS (Dohlen et al. 2008) operating in the K spectral band using the K12 filter pair (wavelength $K1 = 2.110$ µm; wavelength K2=2.251 µm; Vigan et al. 2010) on a circular FOV of ∼5″. For these observations, we also exploited the SPHERE adaptive optics system SAXO (Fusco et al. 2006).

Frames with satellite spots at a symmetrical position with respect to the central star were acquired before and after the science sequence to precisely define the position of the star behind the coronagraph (Langlois et al. 2013). In addition, observations of the star outside the coronagraph were obtained for photometric calibration using a neutral density filter to avoid saturation.

The data were reduced through the SPHERE data center (Delorme et al. 2017), following the data-reduction and handling pipeline (DRH; Pavlov et al. 2008). In the case of IRDIS, the required calibrations are the creation of the master dark and the master flat-field frames and the definition of the star center. For IFS, the calibration list also includes the definition of the position of each spectrum on the detector, the wavelength calibration, and the application of the instrumental flat that takes into account the different responses of each lenslet of the IFS array.

Speckle subtraction was then applied on the reduced data using both angular differential imaging (ADI; Marois et al. 2006) and spectral differential imaging (SDI; Racine et al. 1999), implementing both the principal components analysis (PCA; Soummer et al. 2012) and the TLOCI algorithm (Marois et al. 2014). The application of these algorithms to the SPHERE case is described in Zurlo et al. (2014) and Mesa et al. (2015) and they are currently applied using the SPHERE consortium pipeline application called SpeCal (Galicher et al. 2018).

## 4. Results

Figure 1 shows the S/N maps obtained for IFS (left panel) and IRDIS (right panel) for each epoch. A point source is visible northeast of the star in both epochs, with a S/N of 8.6 and 9.1 for the IFS detection and 5.1 and 16.1 for IRDIS.

The astrometry of the companion was obtained using the negative planet method (see e.g., Bonnefoy et al. 2011; Zurlo et al. 2014) and is reported in Table 3 for both epochs. The astrometric calibration including the definition of the star center, the pixel scale, and angle of true north (TN), together with their respective errors, are obtained following the strategy devised in Maire et al. (2016).

Figure 2 shows the relative astrometry of the companion candidate. The comparison between the expected position in the second epoch of a background object, represented by a black square, and the measured position of the candidate companion, represented by a violet diamond, clearly shows that the candidate is co-moving with AF Lep. Only the IFS data were used, because of their higher precision compared to the IRDIS values (Zurlo et al. 2014), which does however lead to similar results. The large shift of the foreseen position for a background object between the two epochs is mainly due to a favorable combination of the contributions from proper motion and parallactic motion. In this particular case, the contribution from the latter is more important than that from proper motion.

The IFS projected angular separation of AF Lep b corresponds to a projected physical separation of 9.0 ± 0.1 au in the first epoch and of 8.9 ± 0.1 au in the second epoch. This makes this planet one of the nearest to its host star among those discovered through direct imaging, with a very similar semi-major axis to that of $\beta$ Pic b (see e.g., Brandt et al. 2021a).

The analysis of the measured PMa signal, combined with the information on the astrometry from the SPHERE data, can be used to obtain further confirmation of the co-moving and planetary-mass nature of the detected companion. Using the

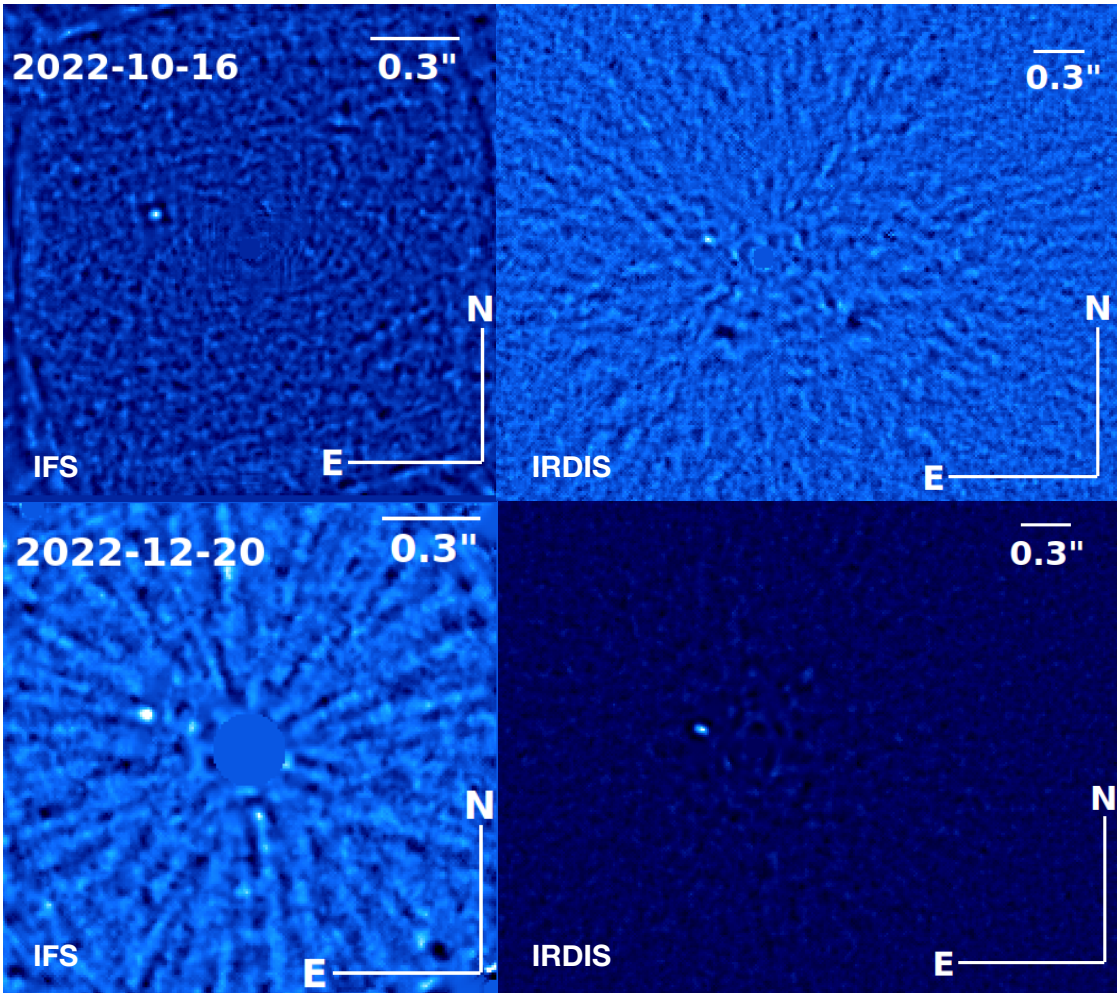


**Fig. 1.** Final S/N maps both for IFS (left panels) and IRDIS (right panels) and for both epochs. The images for the October 16, 2022, epoch are in the upper panels while those for the December 20, 2022, epoch are in the lower panels. For both epochs, the IFS images are obtained by applying a PCA with 150 principal components, while in the IRDIS case, we adopted just 5 principal components. The low-mass companion is clearly visible in all the images northeast of the star.

**Table 3.** Astrometric results for AF Lep b obtained from both IFS and IRDIS in both observing epochs.

| | Date | Sep. RA | Err. Sep RA | Sep. Dec. | Err. Sep. Dec. | Sep. tot. | Err. Sep. tot. | PA | Err. PA |
|---|---|---|---|---|---|---|---|---|---|
| IFS | 2022-10-16 | 0.315″ | 0.002″ | 0.113″ | 0.001″ | 0.335″ | 0.002″ | 70.2° | 0.2° |
| IRDIS | 2022-10-16 | 0.314″ | 0.002″ | 0.110″ | 0.002″ | 0.334″ | 0.003″ | 70.7° | 0.3° |
| IFS | 2022-12-20 | 0.314″ | 0.003″ | 0.109″ | 0.004″ | 0.332″ | 0.004″ | 70.9° | 0.9° |
| IRDIS | 2022-12-20 | 0.317″ | 0.004″ | 0.110″ | 0.001″ | 0.335″ | 0.004″ | 70.8° | 0.4° |

FORECAST algorithm (Finely Optimised REtrieval of Companions of Accelerating STars[2], see Bonavita et al. 2022 for a detailed description), we were able to identify the region where a companion compatible with the measured PMa should appear in the IFS FOV based on the PA of the PMa vector reported in Table 2. FORECAST evaluates the position angle of each pixel in the IFS image with respect to the center and then compares it with the measured value of the PA, identifying an optimal region on the image whilst also taking into account the possible orbital motion of a companion at that position between the SPHERE observation and the *Gaia* observations. Finally, FORECAST also associates a value of the companion mass to each point of the resulting 2D map based on the PMa absolute value, which is calculated using the approach from Kervella et al. (2019). The resulting 2D map is shown in Fig. 3, with the position of the companion perfectly within the optimal region and shown as a red circle; this position corresponds to a dynamical mass of ~5.5 $M_{\rm Jup}$.

The negative planet method was also used to extract the photometry of the companion from each wavelength channel of both IFS and IRDIS. In the first epoch, the IFS channels in Y spectral band are largely dominated by the noise and it was not possible to extract any reliable results. In any case, it was possible to obtain reliable photometric results in J, H, K1, and K2 spectral

[2] https://maps.exoplanetsforecast.com/

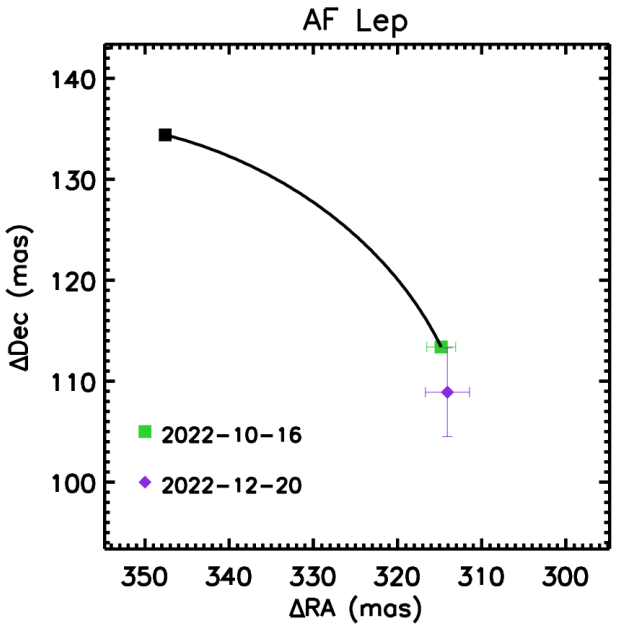


**Fig. 2.** Relative astrometry plot for the candidate companion of AF Lep. The green square represents the relative position of the companion at the first observing epoch, while the violet diamond represents the relative position of the companion at the second epoch. The solid black line represents the expected motion relative to the host star of a background object, while the black square is the expected position for a background object at the epoch of the second observation.

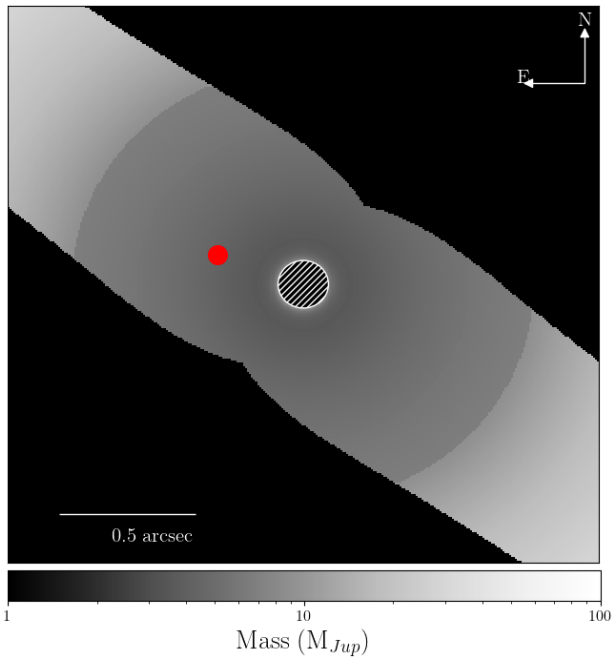


**Fig. 3.** Two-dimensional maps obtained with FORECAST, showing the sky area compatible with the PMa reported in Table 1 in gray. The intensity of the gray areas changes according to the dynamical mass (in $M_{\rm Jup}$) responsible for the PMa at a given distance, with the scale given by the lower color bar. The position of AF Lep b for the first SPHERE epoch is shown as a red circle. We do not plot the position of the companion in the second epoch in order to avoid overlapping between the two positions.

**Table 4.** IFS and IRDIS photometry of AF Lep b from both observing epochs.

| Sp. band | Date | Δmag | Abs. mag. | Mag error |
|---|---|---|---|---|
| Y | 2022-10-16 | – | – | – |
| J | 2022-10-16 | 14.38 | 17.50 | 0.77 |
| H | 2022-10-16 | 13.88 | 16.82 | 0.61 |
| K1 | 2022-10-16 | 11.56 | 14.34 | 0.26 |
| K2 | 2022-10-16 | 11.88 | 14.66 | 0.55 |
| Y | 2022-12-20 | 14.09 | 17.21 | 0.61 |
| J | 2022-12-20 | 13.95 | 17.07 | 0.33 |
| H | 2022-12-20 | 13.52 | 16.46 | 0.36 |
| K1 | 2022-12-20 | 11.70 | 14.48 | 0.07 |
| K2 | 2022-12-20 | 11.79 | 14.57 | 0.07 |

**Table 5.** Mass estimates for AF Lep b obtained from the photometry listed in Table 3 and adopting the AMES-COND atmospheric models.

| Sp. band | Date | Mass ($M_{\rm Jup}$) | Err. Mass ($M_{\rm Jup}$) |
|---|---|---|---|
| Y | 2022-10-16 | – | – |
| J | 2022-10-16 | 2.19 | 0.14 |
| H | 2022-10-16 | 2.37 | 0.19 |
| K1 | 2022-10-16 | 4.14 | 0.34 |
| K2 | 2022-10-16 | 5.68 | 0.40 |
| Y | 2022-12-20 | 2.76 | 0.20 |
| J | 2022-12-20 | 2.40 | 0.19 |
| H | 2022-12-20 | 2.72 | 0.19 |
| K1 | 2022-12-20 | 4.02 | 0.28 |
| K2 | 2022-12-20 | 5.80 | 0.41 |

bands in the first epoch and for all the spectral bands during the second epoch. These results are listed in Table 4. The extracted photometry was then used to obtain a first estimate of the mass of the companion using the AMES-COND atmospheric models (Allard et al. 2003). The resulting values are listed in Table 5 and range between ∼2 and ∼5.5 $M_{\rm Jup}$, placing AF Lep b among the least massive planets detected with direct imaging so far. Using the same models, we can also estimate the radius of the companion, obtaining values ranging between 1.30 and 1.35 $R_{\rm Jup}$.

Using the same procedure used for the photometry of the companion, we were also able to extract a low-resolution spectrum, combining IFS (orange squares) and IRDIS (blue squares) data, making a weighted mean over the two epochs. The resulting spectrum is shown in Fig. 4. The results from the two epochs are in good agreement for the H and the K spectral bands, while the agreement is less good for the Y and J spectral bands. This is due to the fact that the Y band data for the first epoch are completely dominated by noise, while this was not true in the second epoch. The difference is less important in the J band, but the peak – clearly visible in both epochs – has an intensity in the second epoch that is just 65% in flux with respect to that in the first epoch. For this reason, the result in these spectral bands should be taken with some care. Finally, the spectral region around 1.4 µm, which is affected by the presence of water telluric absorption, was also excluded from the extracted spectrum.

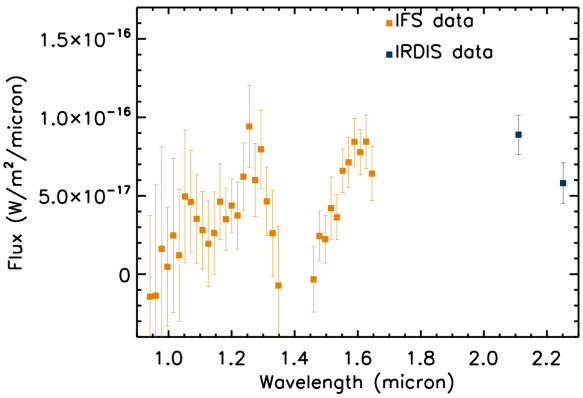


**Fig. 4.** Extracted spectrum for AF Lep b using both IFS and IRDIS data. Each data point is obtained by calculating the mean of the values obtained in the two observing epochs. The orange squares are the IFS data points while the blue ones are the IRDIS data points.

## 5. Discussion

In Sect. 5, we present the detection of a low-mass candidate companion in both our SPHERE observations of AF Lep, which was retrieved with a S/N above 8–9 in the IFS data and a S/N of just 5 in the first epoch of IRDIS data and of 16.1 in the second. Although the conditions were suboptimal in both epochs, the characteristics of the candidate, combined with the additional information provided by the measured HIPPARCOS-*Gaia* eDR3 PMa, are such that we are confident that the detection is genuine.

Indeed, the separation and the position angle for AF Lep b are coherent in all the observations, and so we are in no doubt that we are observing a real object and not a badly subtracted speckle. The differences in the position of the companion between the two epochs could be regarded as orbital motion, even though it is difficult to draw a definitive conclusion on this because of the small time span between the two observations. The comparison of the astrometric position of the companion in the two epochs is clear confirmation that the companion is indeed gravitationally bound to the star and is not a background object. Moreover, in this case, we also have astrometric measurements and the PMa signal obtained by Kervella et al. (2022), which further confirm that the object we have found is indeed a bound companion. It is important to note that the position of the detected candidate is coherent with the expected position for an object causing the PMa signal within the uncertainties related to the time elapsed between the *Gaia* and SPHERE epochs. Furthermore, the photometric mass obtained for our candidate is coherent with the dynamical mass expected at that separation to justify the PMa signal. Further follow-up observations will be important to further constrain its orbital and physical characteristics. However, the convergence of different detection methods towards results that are in good agreement with each other allows us to conclude that the detected companion is indeed a bound object.

There are more reasons to exclude that the candidate companion is a background object. First of all, the candidate companion is very red and has a spectrum compatible with being a low-mass physical companion to AF Lep. Secondly, given the large proper motion of the star (about 50 mas a$^{-1}$), if the candidate companion were a background object, it would have been found about 0.9″ southeast of the star at the epoch of the first observation of AF Lep reported by Galicher et al. (2016) in February 2006. At this separation, the limiting contrast of the observations of these latter authors is 13 mag (in the CH4 band) and the candidate companion should have been detected, while it was not. In addition, there are 760 background stars in *Gaia* DR3 with a contrast of <15 mag in the G-band within 10 arcmin from AF Lep. This contrast is comparable to the observed contrast of the candidate companion, which would likely be an M-star if it were a background object. The surface density of background stars is then $6.72 \times 10^{-4}$ stars arcsec$^{-2}$. The probability of finding one of them at 0.335″ or less from AF Lep is therefore $2.3 \times 10^{-4}$. From all these considerations, we can conclude that it is very unlikely that the candidate companion is a background object.

This target has been observed in several high-contrast imaging survey. We therefore consider why it was never detected before. The detection of AF Lep b in our images is due to a combination of the very good sensitivity of SPHERE at short separations and of the epoch when this observation was carried out. Indeed, given the position of AF Lep b and the direction of the PMa vector (PA = 233.5°), and considering the fact that it is almost parallel to the companion's PA (~70°), suggesting a high orbital inclination, the separation between the star and the planet was much smaller in the recent past. Given the absolute value of the PMa and the mass ratio we determined ($q$~0.005), we may roughly estimate that the speed of the planet around the star is currently ~53 mas a$^{-1}$. The planet should then have been very close to the star (separation <0.1″) at the epochs of the most recent observations of AF Lep, as in the ISPY (Launhardt et al. 2020), GPI (Nielsen et al. 2019), LEECH (Stone et al. 2018) campaigns, which were performed between 2014 and 2016. Older observations, such as SPOTS (Asensio-Torres et al. 2018), NICI (Biller et al. 2013), the International Deep planet survey (Galicher et al. 2016), and Kasper et al. (2007), were probably not deep enough to detect this faint object at the small separation at which it lies. In the following sections, we discuss the results obtained for AF Lep b in detail, together with their implications as to the nature of this object.

### 5.1. Spectral fit

To obtain some information on the physical characteristics of AF Lep b, we fitted its spectrum extracted as described in Sect. 4 both to template spectra and atmospheric models. We stress here that these results present a large uncertainty and should be regarded with some care because of the large error bars for each spectral data point, as can be seen in Fig. 4. We obtained the template spectra from the SpexPrism spectral library (Burgasser 2014) and the results of this fitting procedure can be seen in Fig. 5, where we compare the extracted spectrum of AF Lep b with that of the three best-fit template spectra.

The best fit is obtained with ~L6 spectral types, but comparably good fits are obtained for other later L spectra types. We can therefore conservatively conclude that AF Lep b presents a late-L spectral type.

As atmospheric models, we adopted the BT-Settl models (Allard 2014). The results are shown in Fig. 6, where we compare the extracted spectrum of AF Lep b with those of the three best-fit atmospheric models. In this case, the best fits are obtained for models with $T_{\rm eff}$ of between 1300 and 1500 K and surface gravity of $\log g$ ~3.5–4.0 dex. However, in this case also, a larger number of models at different $T_{\rm eff}$ give a comparably good fit. We can therefore assume a relatively large $T_{\rm eff}$ range of between 1000 and 1700 K.

### 5.2. PMa analysis

An alternative way to visualise the results presented above is provided in Fig. 7, which shows the estimated mass of the object

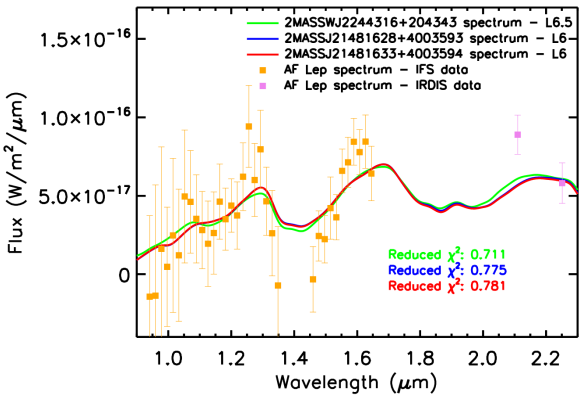


**Fig. 5.** Comparison of the extracted spectrum of AF Lep b with the three best-fit template spectra from the SpexPrism spectral library. The IFS data points are orange squares, while the IRDIS data points are violet squares. The best three template spectra are represented by the green, blue, and red solid lines; they partially overlap with each other. The reduced $\chi^2$ for each template spectrum is reported with the corresponding color.

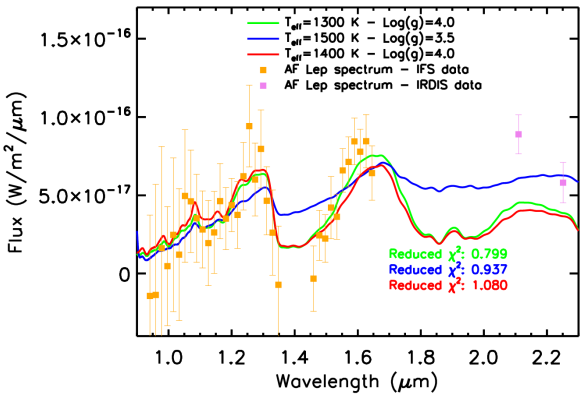


**Fig. 6.** Comparison of the extracted spectrum of AF Lep b with the three best-fit BT-Settl atmospheric models. The IFS data points are shown as orange squares, while the IRDIS data points are shown as violet squares. The best three atmospheric models are represented by the green, blue, and red solid lines. The reduced $\chi^2$ for each atmospheric model is reported with the corresponding color.

causing the PMa signal as a function of the separation from the host star (solid blue line), derived once again following the approach by Kervella et al. (2019). The mass limits obtained from the SPHERE direct-imaging data are also shown for different ages of the system, highlighting that the SPHERE images would have allowed for the detection of any companion compatible with PMa at separations of lower than 4 au. The position of AF Lep b is marked by a red circle, and very good agreement can be seen between the mass obtained from the photometry and the PMa dynamical mass prediction at the separation of the companion.

### 5.3. Orbital fit and dynamical mass estimate

We used the orvara[3] (Orbits from Radial Velocity, Absolute, and/or Relative Astrometry; Brandt et al. 2021b) tool to combine the SPHERE astrometry for our two epochs and the PMa information, and to perform a first orbital fit for AF Lep b. Here, we can obtain a more precise estimate of its dynamical mass.

[3] https://github.com/t-brandt/orvara

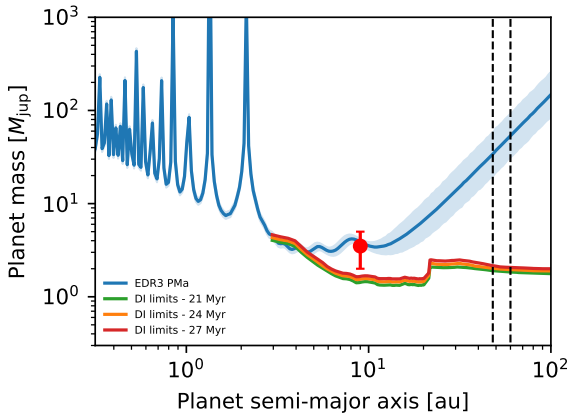


**Fig. 7.** Comparison of the direct imaging results obtained from the SPHERE observations with the PMa results. The solid blue line represents the mass of the object causing the PMa signal as a function of the separation from the host star. The shaded blue area represents the $1\sigma$ confidence interval for this measure. The mass limits obtained from the SPHERE observations for the minimum, expected, and maximum ages are represented by the green, orange, and red solid lines, respectively. The red circle represents the position of AF Lep b on this diagram. The error bar in separation is too small to be shown. The two vertical black dashed lines represent the position of the external belt of the debris disk hosted by AF Lep.

**Table 6.** Summary of the physical and orbital parameters of AF Lep b.

| Parameter | Value |
|---|---|
| Temperature (K) | 1000–1700 |
| Spectral type | Late L (>L6) |
| Photometric mass ($M_{\rm Jup}$) | 2–5.5 |
| Dynamical mass from PMa ($M_{\rm Jup}$) | ~5.5 |
| Dynamical mass from orvara ($M_{\rm Jup}$) | $5.237^{+0.085}_{-0.10}$ |
| Primary mass from orvara ($M_\odot$) | $1.201^{+0.058}_{-0.056}$ |
| Mass ratio | $0.00416^{+0.00022}_{-0.00021}$ |
| Projected separation (arcsec) | 0.334±0.001 |
| Position angle (deg) | 70.65±0.26 |
| Inclination (deg) | $82^{+22}_{-23}$ |
| Semi-major axis (au) | $7.99^{+0.85}_{-0.92}$ |
| Ascending node (deg) | $249^{+16}_{-12}$ |
| Eccentricity | $0.47^{+0.17}_{-0.13}$ |
| Period (yr) | $20.6^{+3.4}_{-3.5}$ |
| Argument of periastron (deg) | $46.4^{+9.3}_{-8.9}$ |
| $T_0$ (JD) | $2456328^{+1386}_{-503}$ |

The results of the fit are summarized by the corner plot shown in Fig. 8 and the best-fit values are reported in Table 6 together with the physical parameters for the companion derived from the spectral fit in Sect. 5.1.

Overall, the results of the fit agree with the estimates of the mass and orbital parameters discussed in the previous section. In particular, the inclination is indeed rather high, corroborating our discussion about the previous non-detections of the companion, and the mass agrees with both the value obtained from the photometry and that resulting from the PMa-only analysis. This once again reinforces our conclusion as to the genuine co-moving nature of the companion.

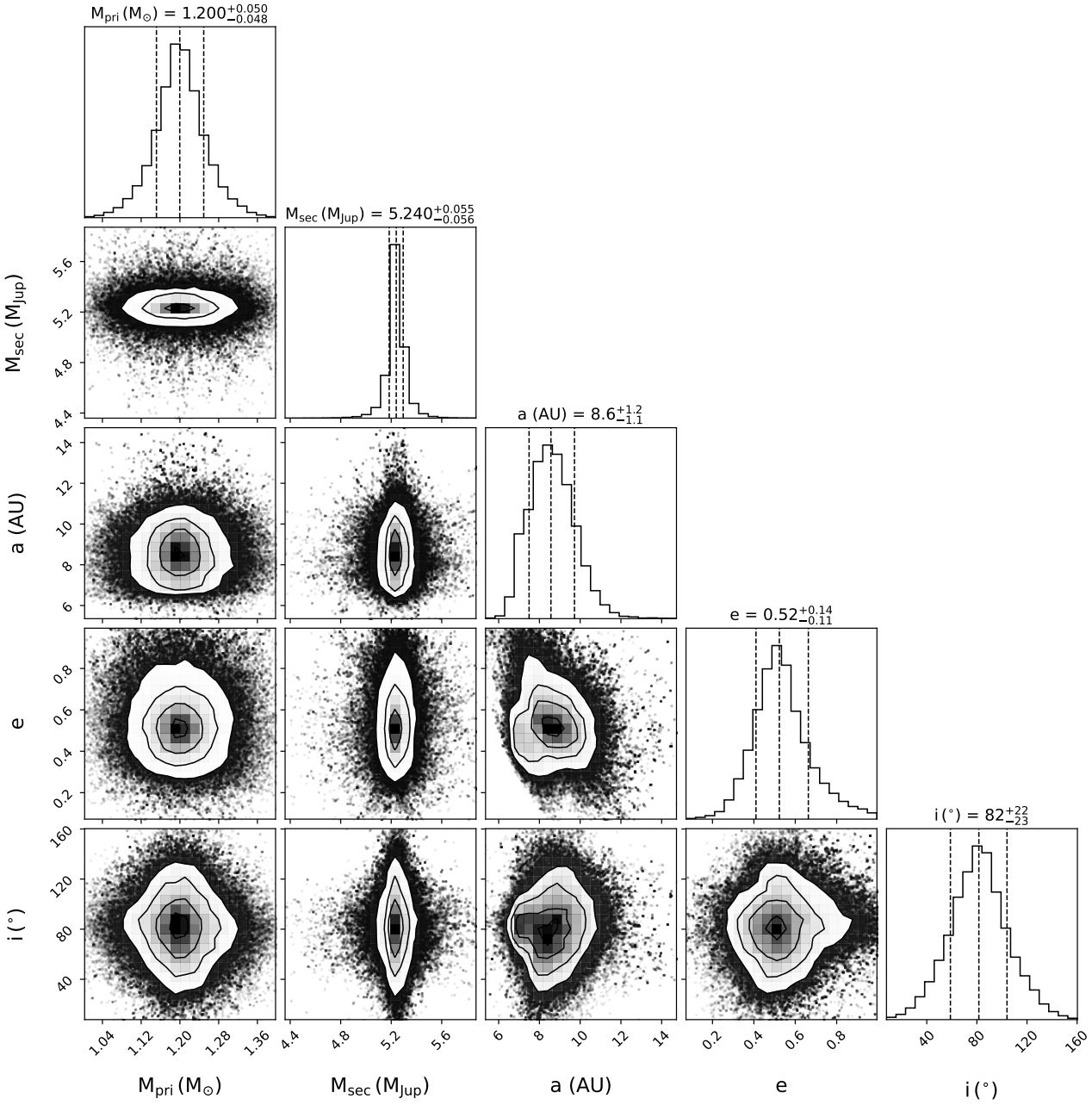


**Fig. 8.** Corner plot showing the results of the orbital fit performed with the orvara tool. The best-fit values are reported in Table 6.

## 6. Conclusion

In this paper, we present near-infrared VLT/SPHERE observations of the nearby, young star AF Lep. The main result of this work is the discovery of a planetary-mass companion at low separation from the star. The measured separation of the companion from the star is of ∼0.335″ corresponding to ∼9 au. We confirm that it is gravitationally bound to its host star by comparing its position relative to the host star in two different epochs. Moreover, further confirmation was possible thanks to astrometric considerations based on the PMa measured for the host star. Using the orvara tool, we derived the orbital parameters compatible with the SPHERE astrometry at the two epochs, as well as with the direction and amplitude of the PMa signature. We were also able to derive a first estimate of the companion's dynamical mass, ∼5.2 $M_{\rm Jup}$, which is in good agreement with the value obtained from the analysis of the PMa alone (5.5 $M_{\rm Jup}$) as well as with the 2–5 $M_{\rm Jup}$ value obtained from the SPHERE photometry using atmospheric models.

The S/N of the detection is generally relatively low, ranging between ∼5 and ∼16 according to the observing epoch and to the instrument used. This is especially true in the Y and J spectral bands for which we obtained large error bars. This partially hampers our capability to extract information from the low-resolution spectrum obtained from SPHERE. In any case, we can conservatively conclude that AF Lep b is a late-L spectral type object with a $T_{\rm eff}$ ranging between 1000 and 1700 K. Observing this target in better weather conditions could allow a detection with a higher S/N, which would enable the extraction of a less noisy spectrum and allow more precise physical characteristics to be obtained.

Finally, it should be noted that AF Lep b is the first companion with a mass well below the deuterium-burning limit detected around a star showing an astrometric signature and

among the smallest directly imaged companions overall. Most of the other directly imaged companions to accelerating stars have masses predominantly in the brown dwarf regime (see e.g., HIP 21152 B, HIP 29724 B, HIP 60584 B and HIP 63734 B Bonavita et al. 2022). The recently discovered planetary-mass companions to HIP 99770 (Currie et al. 2022) and HD 206893 (HD 206893 c; Hinkley et al. 2023) are still more massive than AF Lep b (∼16 $M_{\rm Jup}$ and ∼12.7 $M_{\rm Jup}$, respectively).

Given its mass and separation, and the host star spectral type, AF Lep b can be considered the first directly detected Jupiter analog orbiting an accelerating star. Its resemblance to the Solar System, including the presence of a debris belt at a separation of up to ∼60 au – resembling the Kuiper belt –, makes the AF Lep system an ideal target for future in-depth characterization with GRAVITY or JWST to further refine physical and orbital characteristics of AF Lep b, and with future more precise instruments to search for additional companions.

*Acknowledgements.* This work has made use of the SPHERE Data Center, jointly operated by OSUG/IPAG (Grenoble), PYTHEAS/LAM/CeSAM (Marseille), OCA/Lagrange (Nice) and Observatoire de Paris/LESIA (Paris). This work has made use of data from the European Space Agency (ESA) mission *Gaia* (https://www.cosmos.esa.int/gaia), processed by the *Gaia* Data Processing and Analysis Consortium (DPAC, https://www.cosmos.esa.int/web/gaia/dpac/consortium). Funding for the DPAC has been provided by national institutions, in particular, the institutions participating in the *Gaia* Multilateral Agreement. This research has made use of the SIMBAD database, operated at CDS, Strasbourg, France. D.M., R.G., and S.D. acknowledge the PRIN-INAF 2019 "Planetary systems at young ages (PLATEA)" and ASI-INAF agreement n.2018-16-HH.0. A.Z. acknowledges support from the FONDECYT Iniciación en investigación project number 11190837 and ANID – Millennium Science Initiative Program – Center Code NCN2021_080. S.M. is supported by the Royal Society as a Royal Society University Research Fellow. SPHERE is an instrument designed and built by a consortium consisting of IPAG (Grenoble, France), MPIA (Heidelberg, Germany), LAM (Marseille, France), LESIA (Paris, France), Laboratoire Lagrange (Nice, France), INAF-Osservatorio di Padova (Italy), Observatoire de Genève (Switzerland), ETH Zurich (Switzerland), NOVA (The Netherlands), ONERA (France) and ASTRON (The Netherlands), in collaboration with ESO. SPHERE was funded by ESO, with additional contributions from CNRS (France), MPIA (Germany), INAF (Italy), FINES (Switzerland) and NOVA (The Netherlands). SPHERE also received funding from the European Commission Sixth and Seventh Framework Programmes as part of the Optical Infrared Coordination Network for Astronomy (OPTICON) under grant number RII3-Ct-2004-001566 for FP6 (2004–2008), grant number 226604 for FP7 (2009–2012) and grant number 312430 for FP7 (2013–2016). For the purpose of open access, the authors have applied a Creative Commons Attribution (CC BY) licence to any Author Accepted Manuscript version arising from this submission.

## References

Allard, F. 2014, IAU Symp., 299, 271
Allard, F., Guillot, T., Ludwig, H.-G., et al. 2003, IAU Symp., 211, 235
Asensio-Torres, R., Janson, M., Bonavita, M., et al. 2018, A&A, 619, A43
Bell, C. P. M., Mamajek, E. E., & Naylor, T. 2015, MNRAS, 454, 593
Beuzit, J. L., Vigan, A., Mouillet, D., et al. 2019, A&A, 631, A155
Biller, B. A., Liu, M. C., Wahhaj, Z., et al. 2013, ApJ, 777, 160
Blackwell, D. E., & Lynas-Gray, A. E. 1994, A&A, 282, 899
Bonavita, M., Fontanive, C., Gratton, R., et al. 2022, MNRAS, 513, 5588
Bonnefoy, M., Lagrange, A. M., Boccaletti, A., et al. 2011, A&A, 528, A15
Brandt, T. D. 2018, ApJS, 239, 31
Brandt, T. D. 2021, ApJS, 254, 42
Brandt, G. M., Brandt, T. D., Dupuy, T. J., Li, Y., & Michalik, D. 2021a, AJ, 161, 179
Brandt, T. D., Dupuy, T. J., Li, Y., et al. 2021b, AJ, 162, 186
Burgasser, A. J. 2014, ASI Conf. Ser., 11, 7
Butler, R. P., Vogt, S. S., Laughlin, G., et al. 2017, AJ, 153, 208
Chauvin, G., Desidera, S., Lagrange, A. M., et al. 2017a, in SF2A-2017: Proceedings of the Annual Meeting of the French Society of Astronomy and Astrophysics, eds. C. Reylé, P. Di Matteo, F. Herpin, E. Lagadec, A. Lançon, Z. Meliani, & F. Royer, 331
Chauvin, G., Desidera, S., Lagrange, A. M., et al. 2017b, A&A, 605, L9
Claudi, R. U., Turatto, M., Gratton, R. G., et al. 2008, SPIE Conf. Ser., 7014, 70143E
Currie, T., Brandt, G. M., Brandt, T. D., et al. 2022, Science, submitted [arXiv:2212.00034]
Cutispoto, G., Tagliaferri, G., Pallavicini, R., Pasquini, L., & Rodono, M. 1996, A&AS, 115, 41
Cutri, R. M., Skrutskie, M. F., van Dyk, S., et al. 2003, VizieR Online Data Catalog: II/246
Delorme, P., Meunier, N., Albert, D., et al. 2017, in SF2A-2017: Proceedings of the Annual meeting of the French Society of Astronomy and Astrophysics, eds. C. Reylé, P. Di Matteo, F. Herpin, E. Lagadec, A. Lançon, Z. Meliani, & F. Royer, 347
De Rosa, R. J., Nielsen, E. L., Wahhaj, Z., et al. 2023, A&A, 672, A94
Desidera, S., Chauvin, G., Bonavita, M., et al. 2021, A&A, 651, A70
Dohlen, K., Langlois, M., Saisse, M., et al. 2008, SPIE Conf. Ser., 7014, 70143L
Eggen, O. J. 1986, AJ, 92, 910
Eker, Z., Ak, N. F., Bilir, S., et al. 2008, MNRAS, 389, 1722
Evans, T. M., Ireland, M. J., Kraus, A. L., et al. 2012, ApJ, 744, 120
Franson, K., Bowler, B. P., Bonavita, M., et al. 2023a, AJ, 165, 39
Franson, K., Bowler, B. P., Zhou, Y., et al. 2023b, ApJL, submitted [arXiv:2302.05420]
Fusco, T., Rousset, G., Sauvage, J. F., et al. 2006, Opt. Express, 14, 7515
Gaia Collaboration (Brown, A. G. A., et al.) 2021, A&A, 649, A1
Gaia Collaboration (Vallenari, A., et al.) 2023, A&A, in press, https://doi.org/10.1051/0004-6361/202243940
Galicher, R., Marois, C., Macintosh, B., et al. 2016, A&A, 594, A63
Galicher, R., Boccaletti, A., Mesa, D., et al. 2018, A&A, 615, A92
Gray, R. O., Corbally, C. J., Garrison, R. F., et al. 2006, AJ, 132, 161
Groff, T. D., Kasdin, N. J., Limbach, M. A., et al. 2015, SPIE Conf. Ser., 9605, 96051C
Haffert, S. Y., Bohn, A. J., de Boer, J., et al. 2019, Nat. Astron., 3, 749
Hinkley, S., Lacour, S., Marleau, G. D., et al. 2023, A&A, 671, L5
Høg, E., Fabricius, C., Makarov, V. V., et al. 2000, A&A, 355, L27
Järvinen, S. P., Arlt, R., Hackman, T., et al. 2015, A&A, 574, A25
Kasper, M., Apai, D., Janson, M., & Brandner, W. 2007, A&A, 472, 321
Keppler, M., Benisty, M., Müller, A., et al. 2018, A&A, 617, A44
Kervella, P., Arenou, F., Mignard, F., & Thévenin, F. 2019, A&A, 623, A72
Kervella, P., Arenou, F., & Thévenin, F. 2022, A&A, 657, A7
Kim, Y.-C., & Demarque, P. 1996, ApJ, 457, 340
Langlois, M., Vigan, A., Moutou, C., et al. 2013, in Proceedings of the Third AO4ELT Conference, eds. S. Esposito, & L. Fini, 63
Langlois, M., Gratton, R., Lagrange, A. M., et al. 2021, A&A, 651, A71
Launhardt, R., Henning, T., Quirrenbach, A., et al. 2020, A&A, 635, A162
Macintosh, B., Graham, J. R., Ingraham, P., et al. 2014, PNAS, 111, 12661
Macintosh, B., Graham, J. R., Barman, T., et al. 2015, Science, 350, 64
Maire, A.-L., Langlois, M., Dohlen, K., et al. 2016, SPIE Conf. Ser., 9908, 990834
Marois, C., Lafrenière, D., Doyon, R., Macintosh, B., & Nadeau, D. 2006, ApJ, 641, 556
Marois, C., Correia, C., Véran, J.-P., & Currie, T. 2014, IAU Symp., 299, 48
Marsden, S. C., Mengel, M. W., Donati, F., et al. 2006, ASP Conf. Ser., 358, 401
Marsden, S. C., Petit, P., Jeffers, S. V., et al. 2014, MNRAS, 444, 3517
Mesa, D., Gratton, R., Zurlo, A., et al. 2015, A&A, 576, A121
Messina, S., Lanzafame, A. C., Malo, L., et al. 2017, A&A, 607, A3
Nielsen, E. L., De Rosa, R. J., Macintosh, B., et al. 2019, AJ, 158, 13
Nordström, B., Mayor, M., Andersen, J., et al. 2004, A&A, 418, 989
Nowak, M., Lacour, S., Lagrange, A. M., et al. 2020, A&A, 642, A2
Pavlov, A., Feldt, M., & Henning, T. 2008, ASP Conf. Ser., 394, 581
Pawellek, N., Wyatt, M., Matrà, L., Kennedy, G., & Yelverton, B. 2021, MNRAS, 502, 5390
Pecaut, M. J., & Mamajek, E. E. 2013, ApJS, 208, 9
Racine, R., Walker, G. A. H., Nadeau, D., Doyon, R., & Marois, C. 1999, PASP, 111, 587
Soummer, R., Pueyo, L., & Larkin, J. 2012, ApJ, 755, L28
Stone, J. M., Skemer, A. J., Hinz, P. M., et al. 2018, AJ, 156, 286
Tagliaferri, G., Cutispoto, G., Pallavicini, R., Randich, S., & Pasquini, L. 1994, A&A, 285, 272
Vigan, A., Moutou, C., Langlois, M., et al. 2010, MNRAS, 407, 71
Vigan, A., Fontanive, C., Meyer, M., et al. 2021, A&A, 651, A72
Zurlo, A., Vigan, A., Mesa, D., et al. 2014, A&A, 572, A85